

Determination of semiconductor band gap state parameters from photoconductivity measurements. II. Experimental results

C. Longeaud,¹ J. A. Schmidt,² and R. R. Koropecik²

¹Laboratoire de Génie Electrique de Paris, (UMR 8507 CNRS) Ecole Supérieure d'Electricité, Université Paris VI et XI, Plateau de Moulon, 91192 Gif-sur-Yvette CEDEX, France

²INTEC (UNL-CONICET), Güemes 3450, and FIQ (UNL), Santiago del Estero 2829, 3000 Santa Fe, Argentina

(Received 11 October 2005; revised manuscript received 24 February 2006; published 9 June 2006)

In this paper we apply various photoconductivity techniques to study different types of semiconductors. These methods are the modulated photocurrent, the steady-state photocarrier grating, and the steady-state photoconductivity techniques, and they are used to investigate a chromium-doped gallium arsenide crystal and different hydrogenated amorphous silicon thin films. First, we briefly recall what information on the material transport parameters can be extracted from the results of these various techniques. Second, we experimentally put into evidence the links existing between these apparently very dissimilar techniques by applying them first to a GaAs:Cr crystal and finally to three hydrogenated amorphous silicon samples prepared under different conditions. For this latter material, we show that the density of states distribution, the electron capture cross sections of the states—even that of the valence band tail—and the electron extended-states mobility can be obtained from the comparison of the results of these techniques. We conclude by showing that, by introducing these parameters into a numerical simulation, we can reproduce the behaviors experimentally observed for all the photoconductivity techniques.

DOI: [10.1103/PhysRevB.73.235317](https://doi.org/10.1103/PhysRevB.73.235317)

PACS number(s): 73.50.-h, 73.61.Jc, 73.50.Gr

I. INTRODUCTION

Photoconductivity measurements are among the most valuable techniques to explore the optoelectronic properties of photoconductive semiconductors. In a previous paper¹ we have shown that a link between the density of states (DOS) of such semiconductors and the data measured under steady-state photoconductivity (SSPC) could be drawn. Defining a coefficient γ by $\gamma = \delta \ln(\sigma) / \delta \ln(G)$, where σ is the photoconductivity resulting from the dc generation rate G , we derived an expression relating γ to DOS parameters such as the density of states N , the mean capture coefficient of the recombining states C and the extended states mobility μ of the majority carriers.

In the same publication we have also demonstrated that photoconductivity techniques apparently very different are actually rather close to each other, and when applied to the same sample their complementarity can be a very powerful tool for the determination of the transport parameters of a semiconductor. For instance, we have underlined that the calculations related to the modulated photocurrent (MPC) technique²⁻⁵ can be used in a very simple way to obtain an expression of the SSPC γ coefficient. In the same way, the link between the procedure^{6,7} that we have defined to extract the DOS from the steady-state photocarrier grating⁸ (SSPG) technique and the expression of γ was put forward. Finally, we have suggested some experimental procedures to extract as many transport parameters as possible, combining the results of all these techniques.

However, all these developments were just theoretical, and all the possibilities of these techniques have been studied and exemplified only by means of numerical simulations. The aim of the present paper is to experimentally validate this theoretical approach by applying the various techniques to crystalline and amorphous thin film semiconductors.

In Sec. II we will summarize the results of our previous theoretical developments. In Sec. III we will show that these results apply to crystalline semiconductors by presenting results obtained with a chromium-doped gallium arsenide crystal. In Sec. IV our developments will be applied to hydrogenated amorphous silicon (a-Si:H) thin films, and finally we will conclude in Sec. V.

II. THEORETICAL SUMMARY

In this section we recall briefly the experimental procedures used in each of the photoconductive techniques, and we put into evidence the various relations between the transport parameters of a given semiconductor and the experimental data. We also stress the links between these techniques and their complementarity in a keen determination of material properties. For definiteness we shall consider the case of a semiconductor for which electrons are the majority carriers, since the experimental data were obtained on such materials. Therefore we shall assume $\mu_n \tau_n \gg \mu_p \tau_p$, where μ_n (μ_p) is the electron (hole) extended-states mobility and τ_n (τ_p) the free electron (hole) lifetime. However, there is no particular difficulty in studying the case where holes were the majority carriers from the relations presented below.

The SSPC technique consists of measuring the steady state photocurrent or photoconductivity σ , resulting from the illumination of a biased coplanar sample with photons of energy larger than the band gap of the material. In our study of the SSPC technique we have defined a coefficient γ by the relation¹

$$\frac{\delta \sigma}{\sigma} = \gamma \frac{\delta G}{G}. \quad (1)$$

The γ coefficient may depend on the generation rate G , so that the usual proportionality relation $\sigma \propto G^\gamma$ may only be

valid over a limited range of G values. Starting from Eq. (1), after some calculations one ends with

$$\frac{1}{\gamma} - 1 = C_n \tau_n k_B T N(E_{fn}), \quad (2)$$

where k_B is the Boltzmann constant, T is the absolute temperature, $N(E_{fn})$ the density of states at the quasi-Fermi level for electrons E_{fn} , and C_n is a mean value of the capture coefficients of the recombining states (for the definition of this mean value, see Ref. 1). Obviously, if one of the recombining states dominates over the others, C_n corresponds to the capture coefficient of this peculiar defect. By means of Eq. (2) one may expect to achieve a DOS spectroscopy provided that the SSPC experiment is performed at different temperatures or at different generation rates, according to the equation

$$\frac{N(E_{fn})C_n}{\mu_n} = \frac{G}{k_B T \mu_n n} \left[\frac{1}{\gamma} - 1 \right] = \frac{qG}{k_B T \sigma} \left[\frac{1}{\gamma} - 1 \right], \quad (3)$$

the energy scaling being given by

$$E_c - E_{fn} = k_B T \ln \left[\frac{Sq\xi\mu_n N_c}{I_{ph}} \right], \quad (4)$$

where q is the absolute value of the electron charge, ξ the applied electric field, S is the conduction cross-sectional area in which the photocurrent I_{ph} is flowing, and N_c the equivalent density of states at the bottom of the conduction band. A proper energy scaling by means of Eq. (4) requires the knowledge of $\mu_n N_c$.

The modulated photocurrent technique is based on the illumination of a biased coplanar sample by a light flux partially modulated at a pulsation ω . Two quantities are recorded by means of a lock-in amplifier: the modulus of the resulting alternative current $|I_{ac}|$ and its phase shift ϕ referred to the excitation. This experiment can be performed at different temperatures and pulsations under two regimes. One regime, that we call the low-frequency regime (MPC-LF), is such that the recombination of carriers through the gap states dominates the photoconductivity measurements; the other regime, called the high-frequency regime (MPC-HF), is such that the trapping and release of the photogenerated carriers dominates the photoconductivity.

The MPC-LF technique brings the value of $N(E_{fn})$ from the dc generation rate, the temperature, and the slope of the tangent of the phase shift ϕ measured at low ω , following the equation⁵

$$N(E_{fn}) = \frac{2G \tan(\phi)}{k_B T \omega}. \quad (5)$$

The energy scaling uses the same equation as for the γ spectroscopy [Eq. (4)] and thus requires the knowledge of $\mu_n N_c$. In addition, in our previous publication we have demonstrated that at very low pulsations this technique could be used to derive values of γ following the relation

$$\frac{\sigma_{ac}}{\sigma} = \gamma \frac{G_{ac}}{G}, \quad (6)$$

where σ_{ac} is the alternative photoconductivity resulting from the modulated part of the generation rate, G_{ac} .

The above expression closely resembles expression (1) defining γ , in which δG and $\delta \sigma$ have been replaced by G_{ac} and σ_{ac} , respectively. Hence, instead of working under dc conditions with a variable dc flux to measure γ , one can also work with a small ac signal superposed to the dc one, make the frequency very low, and use the ratio of the ac to dc components to calculate γ , and eventually to achieve a DOS spectroscopy. The similarity between Eq. (1) and Eq. (6) underlines the link existing between experiments SSPC and MPC-LF, apparently different.

The MPC-HF technique gives the quantity NC/μ from experimentally known parameters, for instance, the ac generation rate G_{ac} and the modulus of the resulting ac photocurrent I_{ac} , according to the equation^{2,3}

$$\frac{N(E_\omega)C_n}{\mu_n} = \frac{2}{\pi k_B T} Sq\xi G_{ac} \frac{\sin \phi}{|I_{ac}|}. \quad (7)$$

The C_n involved in the MPC-HF- NC/μ is that of the probed states, but a proper energy scaling requires the knowledge of the quantity $C_n N_c$, also called the attempt-to-escape frequency, since E_ω follows from

$$E_c - E_\omega = k_B T \ln \left(\frac{C_n N_c}{\omega} \right). \quad (8)$$

As mentioned in a previous publication, the combination of the MPC-LF and MPC-HF techniques should give an order of magnitude of the ratio C_n/μ_n .⁵ Indeed, the MPC-LF experimentally gives the DOS value N whereas the MPC-HF gives the quantity NC/μ . If in a given energy range both techniques are probing the same states, the ratio C/μ can be deduced from the adjustment of the MPC-LF data to the MPC-HF values.

Finally, the results of the SSPC measurements made under dc illumination can be cross-checked with those of SSPG measurements. The basis of the SSPG experiment consists of illuminating a biased coplanar sample with two laser beams, an intense one of flux F_1 and another one attenuated to a smaller intensity F_2 . If the two beams are coherent and have the same polarization, a light grating develops between the two electrodes with an intensity

$$F(x) = F_1 + F_2 + \gamma_0 2\sqrt{F_1 F_2} \cos \left(\frac{2\pi x}{\Lambda} \right),$$

where x is the space coordinate perpendicular to the electrodes, γ_0 is a factor taking account of the quality of the interferences ($0 < \gamma_0 \leq 1$), and Λ is the grating period. When the two beams do not interfere, the light intensity impinging on the sample is simply $F_0 = F_1 + F_2$, giving rise to a generation rate $G_0 = G_1 + G_2$, and the current density flowing through the sample under the applied electric field is j_0 . In practice, the less intense beam F_2 is chopped at a low frequency so that the current in the sample resulting from this illumination can be easily measured with a lock-in amplifier.

Considering this measurement, without interferences the current is $j_{woi}=j_0-j_1$, where j_1 is the current created by the illumination of the intense beam (F_1) alone. When a light grating is developed on the sample, the signal detected is $j_{wi}=j_0-j_1+\Delta j$. In the standard SSPG experiment the ambipolar diffusion length is deduced from the evolution of $\beta=j_{wi}/j_{woi}$ as a function of Λ .

In recent publications we have shown that it is possible to deduce some part of the DOS distribution, interacting with the *majority* carriers, from the value of β taken at large grating periods (β_{lim}).^{6,7} We obtained the following relation:

$$\frac{N(E_{fn})C_n}{\mu_n} = \frac{qG_0}{k_B T \sigma} \left[\frac{\gamma_0}{(1+G_2/G_1)} \sqrt{\frac{2(1+\gamma G_2/G_1)}{\gamma(1-\beta_{lim})}} - 1 \right], \quad (9)$$

the energy scaling being given by an equation similar to Eq. (4). More recently, we have shown that a link can be drawn between this previous result and the DOS spectroscopy achieved from the SSPC technique.¹ Actually, from the SSPG analysis we have demonstrated that the relation (9) between the quantity NC/μ and the parameter β measured at large grating periods is exactly the same as Eq. (3). In Sec. IV we will show that this behavior is experimentally verified.

In the two following sections we shall show that cross-checking the results of these different techniques applied to the same semiconductors reveals many of the material transport parameters.

III. EXPERIMENTAL RESULTS ON GaAs:Cr

We have first applied some of the techniques briefly described above to a chromium-doped crystal of gallium arsenide (GaAs:Cr). This semi-insulating crystal (activation energy of 0.75 eV) was manufactured at the Institute of Electronic Materials Technology (Warsaw, Poland). A wafer of 400 μm thickness was cut from an ingot grown in the $\langle 100 \rangle$ direction by the liquid encapsulated Czochralski method under B_2O_3 encapsulation. The Hall concentration of free carriers in the GaAs:Cr wafer, measured at 300 K, was $2.2 \times 10^7 \text{ cm}^{-3}$ and the electronic mobility was about $4400 \text{ cm}^2 \text{ V}^{-1} \text{ s}^{-1}$. The chromium concentration, determined by optical absorption at 0.92 eV, was $1.5 \times 10^{16} \text{ cm}^{-3}$. Arrays of coplanar AuGe-Ni ohmic electrodes were formed on the polished surface of the wafer. The gap between electrodes was 0.8 mm. Chips of $4 \times 9 \text{ mm}^2$ in area were cut from the wafer and one of them was mounted on the cold finger of our cryostat.

The MPC-HF technique was performed under IR light ($\lambda=850 \text{ nm}$) with a dc flux of the order of $2 \times 10^{13} \text{ cm}^{-2} \text{ s}^{-1}$ and an ac flux five times lower. The modulation frequencies were in the range 12 Hz–40 kHz. The temperature was varied between 330 K and 100 K in 10 K steps, and the applied field was 500 V/cm.

The SSPC measurements were performed with the same IR light and with fluxes ranging from 1.5×10^{13} to $3 \times 10^{15} \text{ cm}^{-2} \text{ s}^{-1}$. Eight different fluxes were chosen in a 1-2-5 scale ($1 \times 1.5 \times 10^{13}$, $2 \times 1.5 \times 10^{13}$, $5 \times 1.5 \times 10^{13} \text{ cm}^{-2} \text{ s}^{-1}$, ...). The fluxes were measured by placing a

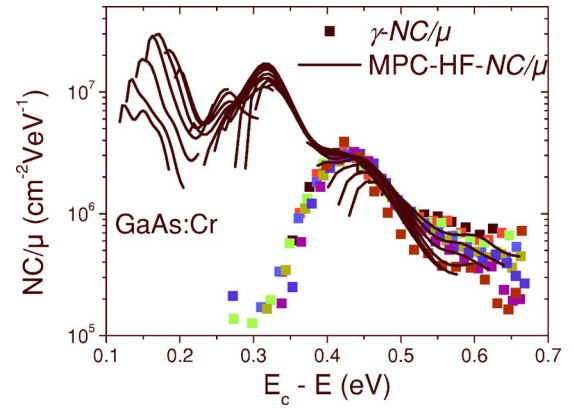


FIG. 1. (Color online) γ - NC/μ (full squares) and MPC-HF- NC/μ (lines) distributions measured on a GaAs:Cr crystal. The two techniques agree rather well to probe a defect peak around 0.43 eV below E_c .

calibrated photodiode in place of the sample. The γ coefficient was measured as a function of flux and temperature over the same range as for the MPC-HF (330–100 K), in 10 K steps. The γ values were obtained from Eq. (1) by using two measurements of the dc currents, at each flux F and at $F \times 1.2$.

It is worth noting that this GaAs:Cr sample has already been studied by the modulated photocurrent, high-resolution photoinduced transient spectroscopy (HRPITS), and transient photocurrent (TPC) techniques.^{9,10} In one of these publications⁹ we have given different methods to derive the energy position and capture coefficient of a given defect state from the analysis of the MPC-HF data. The agreement between all these techniques was rather satisfying and some peak energy positions as well as the corresponding electron capture coefficients were determined for this crystal. In particular, a peak located at 0.43–0.45 eV below the conduction band edge, with a value of $C_n N_c$ of $3\text{--}8 \times 10^{11} \text{ s}^{-1}$, was put into evidence.¹⁰

We present in Fig. 1 the NC/μ distribution obtained from the MPC-HF technique (lines). For this plot the energy scaling, referred to the bottom of the conduction band E_c , was done assuming $C_n N_c = 8 \times 10^{11} \text{ s}^{-1}$ so that the peculiar peak mentioned above is set at its right position (0.44 eV). All the other peaks, detected also by the other techniques (HRPITS and TPC) are also visible, as expected, but their respective position in the plot may be wrong since the energy scaling was done with a $C_n N_c$ parameter that is not the same for all the defects. In the same figure we have plotted the γ - NC/μ distribution resulting from SSPC measurements. To estimate the energy scaling of the γ - NC/μ distribution we adjusted the mobility value to reproduce the energetic position of the peak measured by the MPC-HF technique. The mobility value that resulted, $\mu_n \cong 4400 \text{ cm}^2 \text{ V}^{-1} \text{ s}^{-1}$, is in excellent agreement with the value determined from Hall effect measurements. Moreover, there is no adjustment for the vertical position of the peaks, since both SSPC and MPC-HF provide the NC/μ distribution. Thus, the agreement of the two techniques to describe the same defect peak around 0.44 eV confirms that the SSPC can be used to achieve a DOS spectroscopy of a photoconductive material following the theoretical

developments made in Ref. 1. As already mentioned, the limitation of the SSPC technique is that γ should remain lower than 1. Unfortunately, for the considered crystal we observed that at low temperatures (i.e., low energies), where the splitting of the quasi-Fermi level is large, γ increases rapidly to reach values larger than 1. It seems that some sensitization effect occurs as if a defect level located below midgap, around which the dark Fermi level sits, starts to play a major role in the recombination process. Therefore, the SSPC spectroscopy of the DOS is limited to a single peak for the considered crystal.

Despite this limitation, the experimental results obtained on this GaAs:Cr crystal validate part of the theoretical developments made in Ref. 1. In particular, they show that the matching of the MPC-HF and the SSPC spectroscopies bring some insight to the crystal parameters, such as the capture coefficient of a particular defect and the electrons extended-states mobility.

IV. STUDY OF a-Si:H

A. Experimental results

We have also applied the various photoconductive techniques described in Sec. II to a-Si:H films prepared in radio frequency powered plasma enhanced chemical vapor deposition (rf-PECVD) units under different conditions. One sample (310031) was deposited at 423 K, using a pure silane plasma, a low rf power (≈ 5 mW/cm²), and a low gas pressure (40 mTorr). Another sample (803242) is a polymorphous film deposited at 423 K from a mixture of hydrogen and silane (97% H₂, 3% SiH₄) at a high pressure (1.4 Torr) and a high rf power (110 mW/cm²). Finally, a third sample (PLA158) was deposited at 470 K with dilution of silane into argon (98% Ar, 2% SiH₄) at a pressure of 0.2 Torr and a rf power of 35 mW/cm². The films, deposited on glass, were fitted with two parallel ohmic electrodes with a gap of 1–2 mm. They were annealed under vacuum ($\approx 10^{-5}$ mbar) a few hours at 450 K before measurements.

The MPC-LF was performed illuminating the sample with the light-emitting diode's (LED) red light of 650 nm wavelength at a high dc flux of the order of 3×10^{15} cm⁻² s⁻¹, in a frequency range 1–300 Hz, and varying the temperature in the 100–450 K range in 10 K steps. Two data treatment procedures were applied, a first one in which the DOS was deduced from the slope of $\tan(\phi)$ versus the pulsation ω at low ω values, and a second treatment in which the DOS was deduced from the first *positive* slope of the variation of $\tan(\phi)$ versus ω .

The MPC-HF was achieved with the same red light as for the MPC-LF, with a dc flux of the order of 10^{13} cm⁻² s⁻¹ and an ac flux three times lower. The frequency of the modulation was varied in the range 12 Hz–40 kHz, and the temperature was varied from 450 K to 120 K in 30 K steps.

The SSPC measurements were performed with the same light source, with a flux ranging from 1.5×10^{13} to 3×10^{15} cm⁻² s⁻¹. Eight different fluxes were chosen in a 1-2-5 scale ($1 \times 1.5 \times 10^{13}$, $2 \times 1.5 \times 10^{13}$, $5 \times 1.5 \times 10^{13}$ cm⁻² s⁻¹, ...). The γ coefficient was measured as a

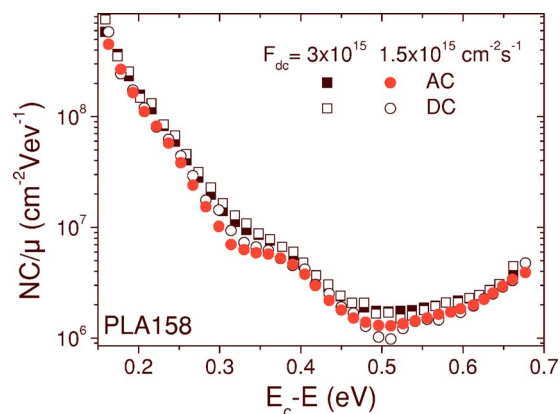


FIG. 2. (Color online) Experimental γ - NC/μ distributions obtained on sample PLA158 (argon diluted) from measurements performed in ac (full symbols) and dc (open symbols) for two different dc fluxes indicated in the figure.

function of temperature—over the same range as in MPC-LF, in 10 K steps—and as a function of flux. The γ values were obtained from Eq. (1) by measuring two dc currents, at each flux F and at $F \times 1.2$. For the highest fluxes we also performed ac measurements, recording I_{ac} with a flux F_{ac} of the order of 20% of the dc flux ($F_{ac} = 0.2 \times F$), and using Eq. (6) to calculate γ .

SSPG, SSPC, and ac photoconductivity measurements were also performed at INTEC (Argentina), using a He-Ne laser ($\lambda = 633$ nm) whose beam was expanded so as to obtain a complete coverage of the sample. For the SSPG measurements, the laser beam was split into two coherent beams. The dc flux impinging the sample was equal to 1.5×10^{16} cm⁻² s⁻¹, whereas the flux of the chopped beam (at $f = 84$ Hz) was 15 times lower. The angle between the two beams was chosen such as to create a grating on the sample with a period of $10.5 \mu\text{m}$, when the two beams were interfering, so that the measured β values were as close as possible to β_{lim} . The β - NC/μ distributions were calculated according to Eq. (9). For the γ measurements in dc, the SSPC was recorded with the full flux of the main beam and with a lower flux obtained by means of a neutral density filter having an optical density of 0.3. The γ - NC/μ distribution was calculated from the dc measurements using Eqs. (1) and (3). From the values of the ac photoconductivity recorded when the two beams were not interfering, we also deduced the ac γ - NC/μ distribution from Eqs. (6) and (3).

The calculations presented in our previous publication¹ predict that we should find the same results in ac and dc for the γ values and thus for the γ - NC/μ distributions. We present in Fig. 2 the distributions calculated either from ac or dc measurements performed at the LGEP (France) on the PLA158 sample with two different light fluxes. The energy scaling was the same for all the curves, using Eq. (4) and assuming a value of 10^{21} cm⁻¹ V⁻¹ s⁻¹ for $\mu_n N_c$. The agreement between the ac and dc curves for the same dc flux is excellent. Of course, we have also checked that this agreement is found for the other samples.

We have also performed “simultaneous” SSPG and photoconductivity (in ac and dc) measurements as function of

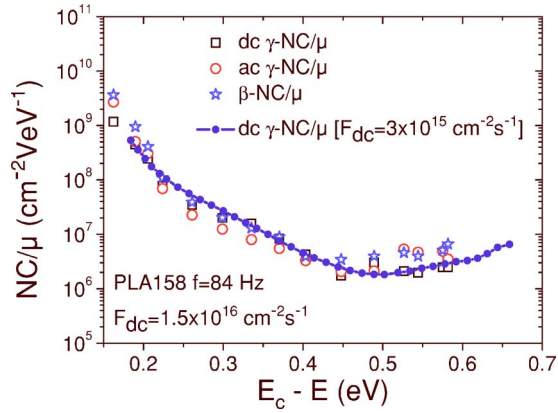


FIG. 3. (Color online) Comparison of various NC/μ distributions obtained on sample PLA158 (Ar diluted). An excellent agreement is obtained between the γ - NC/μ measured in dc (open squares) and in ac (open circles) as well as with the β - NC/μ distribution (open stars). A dc γ - NC/μ distribution obtained with a lower dc flux (line+points), already presented in Fig. 2, also agrees quite well.

temperature on the same sample (PLA158) but in another cryostat at INTEC (Argentina). The different NC/μ distributions are presented in Fig. 3 for which the energy scaling was also achieved with $\mu_n N_c = 10^{21} \text{ cm}^{-1} \text{ V}^{-1} \text{ s}^{-1}$. One can observe the excellent agreement between the γ - NC/μ distributions measured in ac and dc. The very good agreement between the γ - NC/μ and β - NC/μ has been obtained assuming a value of $\gamma_0 = 0.85$. This value is rather close to one and takes into account the diffraction and dispersion of the light by the different optical devices. The ideal value of $\gamma_0 = 1$ would give the same β - NC/μ distribution shape, shifted upwards by a factor of 2. Note also that there is an excellent agreement between the results obtained at INTEC (symbols) with those obtained in LGEP (full line+dots), showing that, for the same sample, the experimental data are perfectly reproducible.

All the above results indicate that we can be rather confident of our theoretical developments,¹ and we have thus performed a DOS spectroscopy combining the results of the MPC-LF, MPC-HF, and SSPC techniques.

We present in Figs. 4–6 the results obtained from the three techniques applied to the three samples. We would like to recall that the interesting part of the MPC-HF data is the upper envelope of the curves, where the points measured at high frequencies for different temperatures are gathering into a single curve. The nature and origin of the “tails” extending below this envelope have already been discussed in many previous papers on this technique, and we will not discuss this further here. One can see that, for all the samples, the MPC-HF envelope gives a curve steadily decreasing with energy, with a large slope at low energies (the conduction band tail region) and a smoother decrease for energies deeper in the gap.

To deduce the DOS and the other parameters, we adjust the MPC-LF and MPC-HF curves one to the other in the conduction band tail (CBT) region, as suggested in Ref. 5. In this zone we expect to have the best coincidence between both methods, since in a narrow energy range close to E_c the

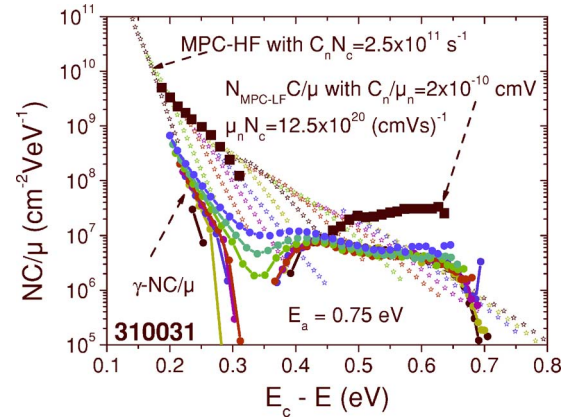


FIG. 4. (Color online) Display of the different NC/μ distributions coming from three different experiments performed on a standard a-Si:H sample: the MPC in the HF regime (stars), the MPC in the LF regime (full squares) and the γ - NC/μ in dc (full circles+lines) obtained for different fluxes, the upper curve corresponding to the highest flux.

CBT is the only species of states to be probed. From this adjustment we deduce the quantities $\mu_n N_c$ (fixing the energy scale of MPC-LF), $C_n N_c$ (defining the energy scale of MPC-HF), and thus the ratio C_n/μ_n . These values can then be applied to all the data. In particular, the γ - NC/μ distribution is plotted with an energy scale that uses the $\mu_n N_c$ found from the MPC-LF results.

The adjustment of the MPC-HF and MPC-LF curves in the CBT region for the three samples give rather similar results, and we have found close values for $\mu_n N_c$, $C_n N_c$, and the ratio C_n/μ_n (see Figs. 4–6). Note that the MPC-HF and MPC-LF NC/μ curves have been plotted on the whole energy range with the values of $C_n N_c$ and C_n/μ_n deduced from this adjustment. The values of these parameters may be improper to plot the MPC-LF and MPC-HF NC/μ distributions for the states deeper than the CBT since the capture coefficients of these states may be different from that of the CBT.

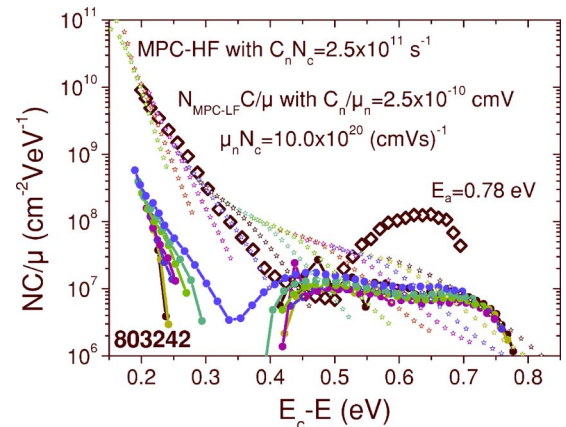


FIG. 5. (Color online) Display of the different NC/μ distributions coming from three different experiments performed on a polymorphous a-Si:H sample: the MPC in the HF regime (stars), the MPC in the LF regime (open diamonds) and the γ - NC/μ in dc (full circles+lines) obtained for different fluxes, the upper curve corresponding to the highest flux.

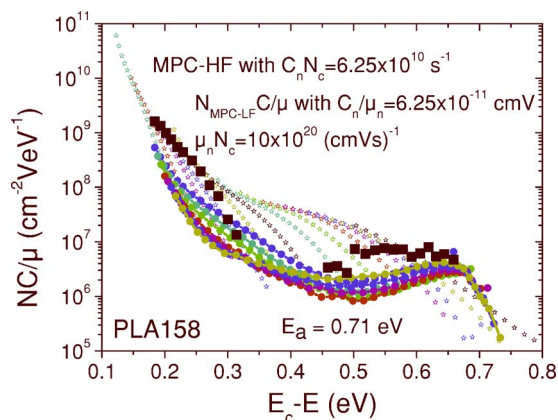


FIG. 6. (Color online) Display of the different NC/μ distributions coming from three different experiments performed on an argon-diluted a-Si:H sample: the MPC in the HF regime (stars), the MPC in the LF regime (full squares) and the γ - NC/μ in dc (full circles+lines) obtained for different fluxes, the upper curve corresponding to the highest flux.

Concerning the γ - NC/μ results, as far as the CBT region is concerned (i.e., at low energies), we can see that, though we have a good agreement between the MPC-HF and MPC-LF data, the γ - NC/μ is approximately a factor of 5 to 15 below. On the other hand, at high energies, for all the samples the γ - NC/μ curves extend up to a certain energy where they drop, corresponding roughly to the energy position of the dark Fermi level E_{f0} . Indeed, at high temperatures the quasi-Fermi level E_{fn} tends towards E_{f0} . One can note that, for samples 803242 and PLA158, there is a good agreement between the measured activation energy of the dark conductivity and the position where the γ - NC/μ curves drop. For sample 310031 there is a slight disagreement (50 meV) that can be explained by a small shift of $E_c - E_f$ with temperature, of the order of 0.1 meV/K, a reasonable value though slightly higher than the ones usually found in the literature.¹¹ Finally, in an intermediate energy range within 0.3 and 0.45 eV, the behavior of the γ - NC/μ depends both on the flux and on the sample. For samples 310031 and 803242 the lowest fluxes give γ values larger than one and consequently, according to Eq. (3), we find unreasonable negative values for γ - NC/μ . For the highest fluxes we find always γ values smaller than 1, but the curves present a minimum. For the sample PLA158 we have always $\gamma < 1$ but the γ - NC/μ distributions obtained at different fluxes present also a minimum around 0.5 eV.

The behavior of the MPC-LF curves in the same energy range (0.3–0.5 eV) depends more on the way the data were treated than on the considered sample. For the samples 310031 and PLA158 we present the MPC-LF DOS as extracted from the first slope of $\tan(\phi)$ versus ω obtained with the lowest values of ω . It appears as an energy range where the MPC-LF DOS is found to be negative because of the sign of the tangent slope. Note that the calculation we had presented in previous papers^{4,5} does not predict the occurrence of a negative slope simply because, for simplicity, we had treated the case of a single species of states. These developments apply rather well when only the CBT states are probed

(for instance, at low temperatures and high fluxes), but the experimental occurrence of a negative slope means that the treatment of the tangent slope has to be refined when one deals with different species of states. This is probably the case for a-Si:H in the energy range 0.3–0.5 eV, where the influence of deep states and band tail states is intermixed. However, this refinement is beyond the scope of the present paper. Moreover, if one uses the first *positive* slope of the tangent then one gets the MPC-LF distribution shown for sample 803242, where a pronounced minimum appears as if only two types of states had to be considered: the CBT states and a distribution of deep states located around midgap. This is in contradiction to the MPC-HF- NC/μ , which seems to give a continuously decreasing distribution of states. Finally, deeper in the gap there is only a limited agreement between the different curves coming from the different techniques.

The discrepancies that we obtain between the different techniques, MPC and SSPC, are in opposition to the agreement we were expecting according to the experimental results exposed in the previous section and at the beginning of this one. As shown in our theoretical development,¹ they certainly come from the fact that each distribution has to be plotted taking into account the proper capture coefficient C ; even for the same distribution, depending on the considered energy range, one may have to take account of a modification of C because the states probed are not the same when changing the temperature or the flux.

B. a-Si:H parameters

If we follow the idea that different C have to be taken into account, we can propose the following interpretation of our experimental results. The easiest discrepancy to explain is the discrepancy between the γ - NC/μ and MPC-HF- NC/μ in the CBT region. We have demonstrated in Ref. 1 that the C that enters into the γ - NC/μ is a mean value of the capture coefficient of the recombining states. At low temperatures, the splitting of the quasi-Fermi levels is such that only two types of states have to be considered: the CBT and the valence band tail (VBT) states. This behavior is due to the fact that both band tails are exponentially increasing towards their respective band edges. Thus, the deep states represent only a small amount of the total number of states in between the quasi-Fermi levels, and at these low temperatures the recombining states to be considered are only the CBT and the VBT states. By means of simulations we have shown that, considering that the electron capture coefficient of the VBT states (C_n^{VBT}) was a factor of 10 below the electron capture coefficients of the CBT states (C_n^{CBT}), the recombination was fully controlled by the VBT because of its larger extent into the gap. Hence, the C involved in the γ - NC/μ data [see Eq. (3)] is that of the VBT states. This results in a NC/μ distribution a factor of 10 below the MPC-HF- NC/μ values, for which the capture coefficient to be considered is that of the probed states, i.e., the CBT states. Considering our experimental results, the ratio between the γ - NC/μ and the MPC-HF- NC/μ distributions gives a good order of magnitude of the ratio C_n^{CBT}/C_n^{VBT} , which takes values between 5 and 15 depending on the sample.

Though we can now explain the experimental results in the CBT region, we still have no explanation for the behavior observed experimentally in the region of the deeper states. For energies in the range 0.5–0.7 eV, just below the Fermi level position, there is a disagreement between all the techniques (see Figs. 4–6). The MPC-LF-NC/ μ distribution plotted with the C of the CBT is much higher than the other distributions. If we bear in mind that the MPC-LF technique gives the N value alone, it means that the C/μ used for this part of the MPC-LF-NC/ μ distribution is probably not appropriate and much too high. It means that around the Fermi level a defect distribution with a rather high density should exist, so that it is seen by the MPC-LF technique, but having a rather low capture coefficient compared to that of the CBT, since these states are not really apparent on the MPC-HF results. We can also add that the MPC-LF-NC/ μ distribution for the deeper energies increases with light soaking,¹² which means that, just above E_{f0} , the MPC technique is probably probing states depending on the hydrogen bonding, as the dangling bonds (DB). To summarize, we suspect that the behavior of the MPC-LF-NC/ μ curves at deep energies is linked to states related to the so-called defect pool.^{13,14} Hence, the ratio between the MPC-HF-NC/ μ and the MPC-LF-NC/ μ plotted with $C=C_n^{CBT}$ gives a good order of magnitude of C_n^{Pool}/C_n^{CBT} . In the very same region one can see that the γ -NC/ μ distribution is not very different from the MPC-HF-NC/ μ distribution. It means that the C involved in the calculation of the γ -NC/ μ and of the MPC-HF-NC/ μ data are not very different. In our previous theoretical paper¹ we have shown that, considering a defect pool density of states, the ratio between the γ -NC/ μ and MPC-HF-NC/ μ distributions was of the same order as the ratio between the capture coefficients of the neutral DB and the positively charged DB. Thus, surprisingly, our results mean that this ratio is not very high, that is less than 10 and more probably close to unity.

Following these interpretations of the experimental results it seems that, by means of the combination of these three techniques, we are then able to *experimentally* get

(i) from the adjustment of the MPC-HF and the MPC-LF distributions at low energies, the $C_n^{CBT}N_c$ parameter for the CBT states as well as the $\mu_n N_c$ value;

(ii) from the MPC-LF data, the density of states shape. This shape is obtained in a plot using the previously determined data (i.e., $C_n^{CBT}N/\mu_n$). Combining these results one can deduce the maximum value of the deep defect density, N_{LF} ;

(iii) from the ratio between the MPC-LF-NC/ μ and the γ -NC/ μ distributions at low energies, the $C_n^{VBT}N_c$ parameter of the valence band tail states;

(iv) from the ratio between the MPC-LF-NC/ μ and the MPC-HF-NC/ μ distributions at deep energies, the average $C_n^{Pool}N_c$ parameter of the midgap recombining states; and

(v) from the ratio between the γ -NC/ μ and the MPC-HF-NC/ μ distributions at deep energies, an order of magnitude of the ratio of the capture coefficients of the positively charged and neutral DB.

The results for all the samples are summarized in Table I, in which we have assumed the value $N_c=2.5 \times 10^{19} \text{ cm}^{-3}$ as for crystalline silicon. This value leads to rather high values

TABLE I. Summary of the values of the density of states parameters determined from the experimental results. The C and μ values have been calculated assuming $N_c=2.5 \times 10^{19} \text{ cm}^{-3}$.

	310031 Std a-Si:H	803242 pm-Si	PLA158 Ar Diluted
$C_{CBT}^n (\text{cm}^3 \text{ s}^{-1})$	1×10^{-8}	1×10^{-8}	2.5×10^{-9}
$N_{LF} (\text{cm}^{-3} \text{ eV}^{-1})$	1.5×10^{17}	6×10^{17}	1.2×10^{17}
$C_{VBT}^n (\text{cm}^3 \text{ s}^{-1})$	2×10^{-9}	5×10^{-10}	8×10^{-10}
$C_{Pool}^n/\mu_n (\text{cm V s})$	2.6×10^{-11}	1.5×10^{-11}	2×10^{-11}
$\mu_n (\text{cm}^2 \text{ V}^{-1} \text{ s}^{-1})$	50	40	40
$C_{Pool}^n (\text{cm}^3 \text{ s}^{-1})$	1.3×10^{-9}	6×10^{-10}	8×10^{-10}

for the mobilities, although still reasonable.¹⁵ Moreover, if one takes a value for N_c three times higher then one ends with electronic extended-states mobility values of the order of 10, commonly quoted in the literature.¹⁶ The capture coefficients are rather low and would be even lower by a factor of 3 if one takes a value of N_c three times higher. Considering the deep defects around midgap, we obtain $C_n^{Pool} \approx 8 \times 10^{-10} \text{ cm}^3 \text{ s}^{-1}$, that is, a capture cross section of the order of $8 \times 10^{-17} \text{ cm}^2$, in good agreement with values proposed by some authors¹⁷ but largely below the value proposed by Lang *et al.* from deep level transient spectroscopy measurements.^{18,19} Indeed, these authors have proposed a value for the attempt-to-escape frequency ($C \times N_c$) of the order of 10^{13} s^{-1} , far above the mean value of $2 \times 10^{10} \text{ s}^{-1}$ that we find. We shall come back to this problem in the next section.

C. Simulation

In Ref. 1 we have presented and extensively used simulations to underline the connections between the different photoconductive techniques experimentally used in this paper. In this section we would like to show that by introducing into one of our simulations the experimental parameters that we have determined, following our interpretation of the data obtained on different samples, it is possible to reproduce all the observed behaviors. Before developing that point we want to discuss an issue raised by our interpretation. Indeed, we have given an interpretation for the results of our measurements in the CBT region and in the deep states region, but we still lack of an interpretation for the narrow range of energies in between these two regions. In Figs. 4–6 we can see that the MPC-LF method provides a rather narrow distribution of DB states for energies just below the dark Fermi level E_{f0} . On one hand, a broad defect pool distribution, extending almost over the whole gap, would result in a rather flat MPC-HF-NC/ μ distribution in the deep states region; see, for instance, Fig. 13 of Ref. 1. However, we observe experimentally that the MPC-HF curves are continuously decreasing with energy. Consequently, the defect pool to be considered is more probably concentrated around the Fermi level. On the other hand, a rather narrow defect pool distribution located around E_{f0} would leave a gap between this distribution and the CBT, and we do not observe such a gap on the MPC-HF experi-

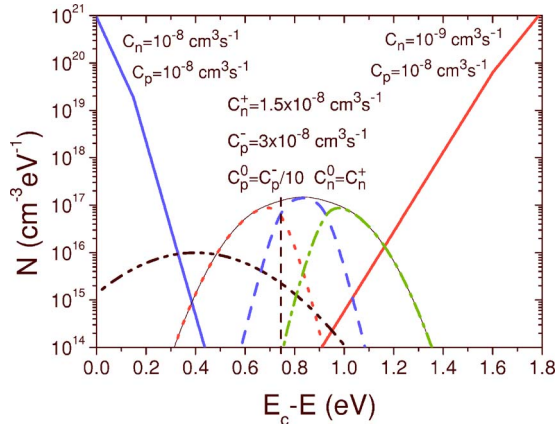


FIG. 7. (Color online) Density of states including a defect-pool distribution of deep defects. The D^+ distribution is shown by the dotted line, the D^0 is shown by the dashed line, and the D^- by the dash-dotted line. The envelope is represented by a thin full line. Acceptor states (dash-dot-dot line) are located in between the CBT and the Fermi level, whose energy position is shown by a vertical dashed line.

mental curves. This region around 0.3–0.5 eV below E_c is probably the more difficult to explore in a-Si:H. Indeed, considering the γ - NC/μ distribution we observe a gap due to the fact that, in this region, the recombination path shifts towards the VBT states, resulting in a γ larger than one. In the same region the MPC-LF- NC/μ distribution also exhibits a gap. If one considers the first slope of $\tan(\phi)$ we obtain negative values for the distribution, and even if we consider the first positive slope of $\tan(\phi)$ we obtain a pronounced minimum in the MPC-LF- NC/μ distribution (see for instance the experimental results for the sample 803242 in Fig. 5). As mentioned above, we do not observe such a gap in the MPC-HF- NC/μ curves, which are steadily decreasing from the CBT states towards the midgap DB states. We believe that a possible solution is to take into account in this region a low density of states, say low enough so that it is not detected by the MPC-LF because it is drowned in the two other distributions (CBT+DB), but with a very high capture coefficient so that the NC/μ quantity matches with the MPC-HF results.

Consequently, we have tried to reproduce the main trends of the experimental curves by means of our simulation, introducing parameters, orders of magnitude of which were taken either from the literature or from our experiments (shown in Table I), plus a very low density of acceptor states with a high capture coefficient. We want to stress that our intention is not to perform a fit of the experimental curves, but rather to show that the experimental main trends can be reproduced with reasonable values for the parameters. A typical DOS introduced in the simulation is shown in Fig. 7. The parameters used in the simulation (and presented below) are summarized in Table II, where those coming from the experiment are written in bold characters. To reproduce the experimental densities we have assumed that the band gap was equal to 1.8 eV. Each band tail is made of two exponential distributions, according to previous results from time of flight experiments.^{20,15} Moreover, for the CBT we had to use

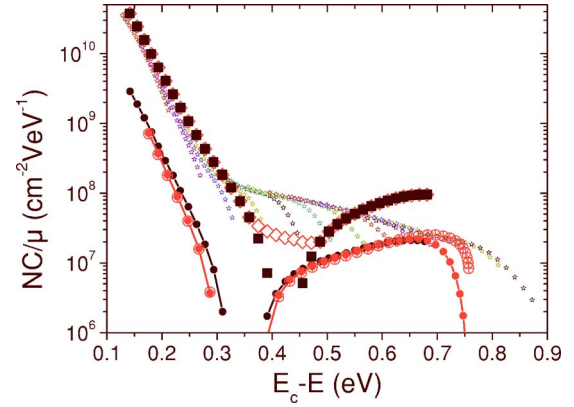


FIG. 8. (Color online) Results of the simulations performed with the DOS shown in Fig. 7. The symbols used are the same as for the experimental curves: MPC-HF (stars), MPC-LF (full squares), γ - NC/μ (line+full circles). The γ - NC/μ upper curve was calculated with the highest generation rate. The open diamonds curve represents the MPC-LF- NC/μ distribution calculated from the first positive slope of $\tan(\phi)$. A β - NC/μ distribution resulting from a SSPG simulation performed with the lowest flux is also shown (crossed open circles) for comparison with the corresponding γ - NC/μ distribution.

two slopes, so that the final NC/μ values in the CBT energy range explored by the experiment and the simulation are approximately of the same order. Assuming a single slope would have resulted in a rather high value for the density of states at the conduction band edge. Indeed, the lower T_c equals 275 K and the CBT-DOS can be extrapolated towards $10^{22} \text{ cm}^{-3} \text{ eV}^{-1}$ at the conduction band edge. At $E_c - E = 0.15 \text{ eV}$ the slope changes and the upper T_c is equal to 440 K, while the DOS reaches $10^{21} \text{ cm}^{-3} \text{ eV}^{-1}$ at E_c (taken as the energy origin). The capture coefficients of the CBT were taken as $C_n^{CBT} = C_p^{CBT} = 10^{-8} \text{ cm}^3 \text{ s}^{-1}$, in agreement with the data of Table I and with the data we proposed a few years ago.^{20,15}

For the VBT we have also used two exponential distributions. Below $E_c - E = 1.6 \text{ eV}$ T_v is equal to 600 K as in device grade materials,²¹ and the exponential DOS can be extrapolated towards $3 \times 10^{21} \text{ cm}^{-3} \text{ eV}^{-1}$ at the valence band edge. For $E_c - E$ in between 1.6 eV–1.8 eV, the upper T_v is 780 K and the DOS reaches $10^{21} \text{ cm}^{-3} \text{ eV}^{-1}$ at E_v . The capture coefficients of the VBT were taken equal to $C_n^{VBT} = 10^{-9} \text{ cm}^3 \text{ s}^{-1}$ and $C_p^{VBT} = 10^{-8} \text{ cm}^3 \text{ s}^{-1}$.

Deane and Powell formalized the notion of defect pool a few years ago.^{22,23} Following their calculations, a defect pool can be introduced in our simulation codes. The proper statistics for correlated states is used to solve the continuity and charge neutrality equations, so that the occupation functions of the different species of states are completely calculated. The various photoconductivity techniques can be then simulated under various experimental conditions. The parameters we have chosen for the pool distribution are as follows: a pool position $E_c - E_{pool} = 0.72 \text{ eV}$, a standard deviation $\sigma_{pool} = 0.11 \text{ eV}$, a hydrogen concentration $[H] = 5 \times 10^{21} \text{ cm}^{-3}$, and a correlation energy $E_u = 0.15 \text{ eV}$, slightly lower than in the simulations of Ref. 1. These data give an integrated density of neutral DB (D^0) of the order of $2.5 \times 10^{16} \text{ cm}^{-3}$ and a

TABLE II. Summary of the parameters introduced in the simulations to reproduce the experimental behaviors. These parameters, or their order of magnitude, come either from the literature data (in italic) or directly from the results of experiments presented herein (in bold).

Parameter	Value
Band gap width	$E_g = 1.8 \text{ eV}$
Equivalent densities of states at E_c and E_v	$N_c = N_v = 6.7 \times 10^{21} * (k_B \times 300)^{3/2} = 2.5 \times 10^{19} \text{ cm}^{-3}$
Extended-states mobilities	Electrons, $\mu_n = 10 \text{ cm}^2 \text{ V}^{-1} \text{ s}^{-1}$ Holes, $\mu_p = 1 \text{ cm}^2 \text{ V}^{-1} \text{ s}^{-1}$
Density of conduction band tail (CBT) states	*For $E_c - E \geq 0.15 \text{ eV}$, $N(E) = 10^{22} \exp[-(E_c - E)/k_B T_{c1}]$ with $T_{c1} = 275 \text{ K}$; *For $0 \leq E_c - E \leq 0.15 \text{ eV}$, $N(E) = 10^{21} \exp[-(E_c - E)/k_B T_{c2}]$, with $T_{c2} = 440 \text{ K}$ $C_n^{\text{CBT}} = 10^{-8} \text{ cm}^3 \text{ s}^{-1}$, $C_p^{\text{CBT}} = 10^{-8} \text{ cm}^3 \text{ s}^{-1}$
Capture coefficients of CBT states	
Density of valence band tail (VBT) states	*For $E_c - E \leq 1.6 \text{ eV}$, $N(E) = 3 \times 10^{21} \exp[-(E_v - E)/k_B T_{v1}]$ with $T_{v1} = 600 \text{ K}$ *For $1.6 \leq E_c - E \leq 1.8 \text{ eV}$, $N(E) = 10^{21} \exp[-(E_v - E)/k_B T_{v2}]$ with $T_{v2} = 780 \text{ K}$ $C_n^{\text{VBT}} = 10^{-9} \text{ cm}^3 \text{ s}^{-1}$, $C_p^{\text{VBT}} = 10^{-8} \text{ cm}^3 \text{ s}^{-1}$
Capture coefficients of VBT states	
Defect pool (DP) parameters	Position, $E_c - E_{\text{pool}} = 0.72 \text{ eV}$ Standard deviation, $\sigma_{\text{pool}} = 0.11 \text{ eV}$ Hydrogen concentration $[H] = 5 \times 10^{21} \text{ cm}^{-3}$ Correlation energy, $E_u = 0.15 \text{ eV}$
Capture coefficients of DP states	$C_n^0 = 1.5 \times 10^{-9} \text{ cm}^3 \text{ s}^{-1}$, $C_p^0 = 3 \times 10^{-9} \text{ cm}^3 \text{ s}^{-1}$, $C_n^+ = C_n^0$, $C_p^- = 10 C_p^0$ $D^0 = 2.5 \times 10^{16} \text{ cm}^{-3}$
Neutral defect density ^a	
Maximum density of gap states ^a	$N_{\text{LF}} = 1.5 \times 10^{17} \text{ cm}^{-3} \text{ eV}^{-1}$
Fermi level position ^a	$E_a = E_c - E_f = 0.755 \text{ eV}$
Additional acceptor states distribution ^b	Position within the gap, $E_c - E = 0.4 \text{ eV}$ Standard deviation, $\sigma = 0.2 \text{ eV}$ Maximum density, $N_{\text{max}} = 10^{16} \text{ cm}^{-3} \text{ eV}^{-1}$ Capture coefficients, $C_n^{\text{Acc}} = 1 \times 10^{-7} \text{ cm}^3 \text{ s}^{-1}$ $C_p^{\text{Acc}} = 1 \times 10^{-8} \text{ cm}^3 \text{ s}^{-1}$

^aDetermined by the previously quoted values of the parameters.

^bThese values give: $\mathbf{NC}_n^{\text{CBT}}/\mu$ (at 0.4 eV) = $1 \times 10^7 \text{ cm}^{-2} \text{ V eV}^{-1}$, in good agreement with the experiment (see Fig. 5).

Fermi level at 0.755 eV below E_c .²¹ The capture coefficients of these states are $C_n^0 = 1.5 \times 10^{-9} \text{ cm}^3 \text{ s}^{-1}$ and $C_p^0 = 3 \times 10^{-9} \text{ cm}^3 \text{ s}^{-1}$, with ratios of 1 for C_n^+ ($C_n^+ = C_n^0$) and 10 for C_p^- ($C_p^- = 10 \times C_p^0$).

We have added an acceptor distribution with $N_{\text{max}} = 10^{16} \text{ cm}^{-3} \text{ eV}^{-1}$ and a standard deviation of 0.2 eV at the position $E_c - E_{\text{acc}} = 0.4 \text{ eV}$. The capture coefficients of these states are $C_n^{\text{Acc}} = 10^{-7} \text{ cm}^3 \text{ s}^{-1}$ and $C_p^{\text{Acc}} = 10^{-8} \text{ cm}^3 \text{ s}^{-1}$. These parameters would give an electron attempt-to-escape frequency of $2.5 \times 10^{12} \text{ s}^{-1}$ and a density of states at the Fermi level of $10^{15} \text{ cm}^{-3} \text{ eV}^{-1}$.

The values of the extended states mobilities were taken equal to $10 \text{ cm}^2 \text{ V}^{-1} \text{ s}^{-1}$ and $1 \text{ cm}^2 \text{ V}^{-1} \text{ s}^{-1}$ for electrons and holes, respectively. We could have taken the values found experimentally ($\approx 40 \text{ cm}^2 \text{ V}^{-1} \text{ s}^{-1}$), but it would not have modified the general trends of the simulation results.

These results are shown in Fig. 8. The MPC-LF was calculated with a generation rate of $4 \times 10^{19} \text{ cm}^{-3} \text{ s}^{-1}$, starting at a frequency of 1 Hz. To calculate MPC-LF- NC/μ we have used either the first four points (full squares) or the first positive slope of $\tan(\phi)$ (open diamonds), and the MPC-LF-

NC/μ was plotted with the capture coefficient of the CBT. The MPC-HF was calculated with a generation rate of $1.3 \times 10^{17} \text{ cm}^{-3} \text{ s}^{-1}$. The $\gamma NC/\mu$ were calculated with these two generation rates. All the experimental behaviors are particularly well reproduced. Therefore, we are quite confident that the DOS parameters extracted from the experimental curves and presented in Table I are excellent orders of magnitude of the true material parameters.

We would like to add a few remarks before concluding. First, in the above DOS two distributions are present around the Fermi level: one with a low capture coefficient and a high density, and a second one with a high capture coefficient and a low density of states. We wonder, and this is only speculative since more work should be done on that point, if, depending on the technique used to probe the states close to the Fermi level, one would see one distribution or the other. This speculation would provide an explanation for the discrepancies on the various attempt-to-escape frequencies found in the literature.¹⁷⁻¹⁹

Note also that to have both the MPC-LF- NC/μ and the $\gamma NC/\mu$ exhibiting a gap we had to take the ratio between the capture coefficients of the D^+ and the D^0 equal to 1 in the

simulation. It does not mean that this value is correct but, if we trust our experimental results and our simulations, it certainly gives a good order of magnitude so that this ratio cannot be larger than a few units.

Finally, since we are dealing with three different capture coefficients for the states' distributions above the Fermi level, it is hard to make a choice for the one to be used to scale the energy in the region probed by the MPC-HF technique. That is why we have made the choice to plot all the MPC-HF data using the CBT capture coefficient, the one that we believe to be the more accurately determined experimentally, though this choice probably enhances the discrepancies between the different curves, especially close to the Fermi level.

V. CONCLUSION

In conclusion, we have experimentally cross-checked the results of different photoconductive techniques that could appear at first sight very different. However, our experimental results underlined the links connecting these techniques. We have shown that SSPG and SSPC measurements lead to the same spectroscopy of the density of states of photoconductive semiconductors. We have also demonstrated that the γ

coefficient can be evaluated either from dc measurements, as from the SSPC technique, or ac measurements, as from the MPC experiment. We have exemplified the complementarity of these techniques to determine DOS or material parameters by investigating the density of states of a crystalline material and of thin a-Si:H films. For this last material we have extracted orders of magnitude for the electron capture coefficients of the different defect states present in the gap, even that of the valence band tail states, by a proper analysis of the data extracted from each of these techniques. By introducing these parameters into numerical simulations, we were able to reproduce all the experimental behaviors observed for the a-Si:H samples. All these results are a good experimental confirmation of all the theoretical developments that were achieved on each of the photoconductive techniques taken independently.

ACKNOWLEDGMENTS

We thank P. Roca I Cabarrocas for providing the standard a-Si:H sample as well as the polymorphous one, P. Chaudhuri for the "argon-diluted" sample, and P. Kaminski for the GaAs:Cr crystal. This work was partially supported by PEI No. 6329 from CONICET and Project No. A02E01 from Ecos Sud-SECyT.

-
- ¹C. Longeaud, J. A. Schmidt, and J. P. Kleider, preceding paper, Phys. Rev. B **73**, 235315 (2006).
²C. Longeaud and J. P. Kleider, Phys. Rev. B **45**, 11672 (1992).
³C. Longeaud and J. P. Kleider, Phys. Rev. B **48**, 8715 (1993).
⁴R. R. Koropecski, J. A. Schmidt, and R. Arce, J. Appl. Phys. **91**, 8965 (2002).
⁵M. E. Gueunier, C. Longeaud, and J. P. Kleider, Eur. Phys. J.: Appl. Phys. **26**, 75 (2004).
⁶J. A. Schmidt and C. Longeaud, Appl. Phys. Lett. **85**, 4412 (2004).
⁷J. A. Schmidt and C. Longeaud, Phys. Rev. B **71**, 125208 (2005).
⁸D. Ritter, E. Zeldov, and K. Weiser, Appl. Phys. Lett. **49**, 791 (1986).
⁹C. Longeaud, J. P. Kleider, P. Kaminski, R. Kozłowski, M. Pawłowski, and J. Cwirko, Semicond. Sci. Technol. **14**, 747 (1999).
¹⁰H. Belgacem, A. Merazga, and C. Longeaud, Semicond. Sci. Technol. **20**, 56 (2005).
¹¹P. Jensen and R. Meaudre, J. Phys.: Condens. Matter **2**, 10411 (1990).
¹²J. P. Kleider, C. Longeaud, and M. E. Gueunier, Phys. Status Solidi C **1**, 1208 (2004).
¹³K. Winer, Phys. Rev. B **41**, 12150 (1990).
¹⁴G. Schumm and G. H. Bauer, Philos. Mag. B **64**, 515 (1991).
¹⁵R. Vanderhaghen, Phys. Rev. B **38**, 10755 (1988).
¹⁶T. Tiedje, in *Semiconductors and Semimetals*, edited by J. Pankove (Academic Press, New York, 1984), pp. 207–238.
¹⁷M. Meaudre and R. Meaudre, J. Phys.: Condens. Matter **13**, 5663 (2001).
¹⁸D. V. Lang, J. D. Cohen, and J. P. Harbison, Phys. Rev. B **25**, 5285 (1982).
¹⁹D. V. Lang, J. D. Cohen, J. P. Harbison, M. C. Chen, and A. M. Sergent, J. Non-Cryst. Solids **66**, 217 (1984).
²⁰C. Longeaud, G. Fournet, and R. Vanderhaghen, Phys. Rev. B **38**(11), 7493 (1988).
²¹M. Stutzmann, Philos. Mag. B **60**, 531 (1989).
²²S. C. Deane and M. J. Powell, Phys. Rev. Lett. **70**, 1654 (1993).
²³M. J. Powell and S. C. Deane, Phys. Rev. B **48**, 10815 (1993).